RSC Advances

ROYAL SOCIETY OF CHEMISTRY

www.rsc.org/advances

RSC Advances

RSCPublishing

ARTICLE

Novel Carbon Nitride Composites with Improved Visible Light Absorption Synthesized in $ZnCl_2$-based Salt Melts†

Cite this: DOI: 10.1039/x0xx00000x

Christian Fettkenhauer,[a] Jens Weber,[b] Markus Antonietti,[a] and Dariya Dontsova*[a]

Received 00th January 2012,
Accepted 00th January 2012

DOI: 10.1039/x0xx00000x

www.rsc.org/advances

Poly(triazine imide)-based carbon nitride materials with the BET surface areas up to 200 m^2/g were synthesized in $ZnCl_2$ containing salt melts without the use of hard templates. We found that composition, structural order, optical properties and morphology of products can be adjusted by careful selection of synthesis parameters. The nature of the salt eutectic and precursor concentration in the melt have an especially large influence, with $ZnCl_2$ being a reactive solvent. This novel synthesis route provides access to easily processable materials with improved optical absorption in the visible range that can be used as composite photocatalysts, CO_2 adsorbents or nanocomposite fillers.

Introduction

Graphitic carbon nitride materials are light element composed polymeric semiconductors which have recently found numerous applications as photo-[1] and electrocatalysts[2], oxidation catalysts[3], catalyst supports and nanocomposite fillers[4], and are reported to be promising even for photovoltaic applications[5]. For most applications, carbon nitrides with a special morphology and relatively high surface areas are needed. Typically, this is achieved by using various silica templates, which need to be removed after the synthesis, mostly by reaction with an HF source[6]. The latter step however requires additional safety precautions and put severe restrictions on scalability of carbon nitrides production. Alternative methods to adjust morphology and surface areas of final products include, for example, supramolecular preorganization of monomers[7], "soft-templating"[8] and solvothermal synthesis[9]. Besides, C_3N_4-related materials such as crystalline poly(triazine imides) (PTI) that have well-defined morphologies and possess increased surface areas can be prepared using LiX/KX salt melts (X=Cl, Br) as reaction media[10].

In general, molten salt(s) can serve as a solvent for high-temperature materials synthesis, as catalyst (for example, $ZnCl_2$ in trimerization reactions) but also as "soft template" for tailoring micro- and mesoporosity of the resulting products. Previously, $ZnCl_2$ and $ZnCl_2$-containing melts were successfully used for the synthesis of porous covalent triazine-based frameworks[11] and porous functional carbons[12].

In this contribution, we further explore the utility of salt melt synthesis for the preparation of carbon nitrides, with the main focus on increasing the surface areas of products, as well as on controlling their structure and morphology by varying the synthesis parameters. We report on the preparation of new carbon nitride hybrid materials using zinc chloride containing eutectic mixtures, their characterization by means of X-ray diffraction (XRD), elemental analysis (EA), X-ray photoelectron spectroscopy (XPS), scanning electron microscopy (SEM), FTIR-spectroscopy and gas adsorption, and discuss potential applications.

Experimental section

Chemicals and materials. Lithium chloride (99 %), sodium chloride (99.5 %), potassium chloride (99 %), cesium chloride (99 %) and Rhodamine B (95 %) were purchased from Sigma Aldrich. Zinc chloride (98 %) was purchased from Alfa Aesar, melamine (99 %) from Acros Organics and dicyandiamide (98 %) from Merck. All the chemicals were used without further purification.

Synthesis procedure. Salts and melamine were ground together in a glovebox (mBraun Unilab , O_2 < 0.1 ppm, H_2O < 0.1 ppm) under argon atmosphere according to the eutectic compositions (Table 1). Reaction mixtures (~5-10 g) were transferred into porcelain crucibles and covered with lids. Crucibles were placed in oven and heated under constant nitrogen flow (15 mL/min). The crude products were removed from the crucibles and washed first with ethanol (50-100 mL), then with deionized water (50-100 mL) and finally with 1M HCl solution (50-100 mL). Each step was carried out for 24 hours. Final products were isolated by filtration, thoroughly washed with deionized water (500 mL) and dried in a vacuum oven at 50 °C for 15 h.

Reference g-C_3N_4 was prepared by heating DCDA with the ramp of 2.3 °C/min up to 550 °C and subsequent holding at this temperature for 4 h under constant nitrogen flow (15 mL/min) in a covered crucible (Scheme S1a). The final product was thoroughly ground.

Dye photodegradation experiments. For photodegradation experiments Rhodamine B (RhB) was used as a model dye. 5 mg of a catalyst were dispersed in 5 mL of RhB solution in

deionized water (10 mg/L) in a cuvette. The suspension was agitated in dark for 30 minutes in order to reach dark-adsorption equilibrium, and then illuminated with a LED module emitting at 420 nm (12 W, OSA Opto Lights) from the fixed distance of 5 cm. The RhB degradation was monitored as the decrease of its concentration over irradiation time using UV/Vis spectrophotometer. For this purpose, after a certain irradiation time *t*, an aliquot of 300 µL of reaction mixture was taken, diluted with 1.7 mL of deionized water, kept for 30 minutes in dark to allow for catalyst precipitation, then UV-Vis absorption spectra were measured. For calculation of the rate constants, dye absorbance (at 550 nm) after dark equilibration (t=0 min), I_0, and at *t*=60 min, *I*, were used. Rate constants *k* were calculated as follows:

$k = ln(I/I_0)*(60\ min)^{-1}$

Characterization. Powder X-Ray diffraction patterns were measured on a Bruker D8 Advance diffractometer with $Cu_{K\alpha}$ radiation (λ = 0.15148 nm) equipped with a scintillation counter detector applying a step size 0.05° 2θ and counting time of 3s per step. FT-IR spectra were recorded on a Varian1000 FT-IR spectrometer equipped with an attenuated total reflection unit with diamond applying a resolution of 4 cm^{-1}. Nitrogen adsorption/desorption measurements were performed after degassing the samples at 150 °C for 20 hours using a Quantachrome Quadrasorb SI-MP porosimeter at 77.4 K. CO_2 and N_2 adsorption/desorption isotherms at 273, 283 and 303 K were conducted on a Quantachrome Autosorb-1MP instrument after prior degassing. The specific surface areas were calculated by applying the Brunauer-Emmett-Teller (BET) model to adsorption isotherms (N_2 at 77.4 K) for $0.05 < p/p_0 < 0.3$ using the QuadraWin 5.05 software package. Elemental analysis was accomplished as combustion analysis using a Vario Micro device. SEM images were obtained on a LEO 1550-Gemini microscope. Optical absorbance spectra of powders were measured on a Shimadzu UV 2600 equipped with an integrating sphere. The absorption spectra of RhB solutions were recorded on a T70 UV/VIS spectrophotometer (PG instruments Ltd.). The emission spectra were recorded on LS-50B, Perkin Elmer instrument. The excitation wavelength was 300 nm. EDX investigations were conducted on a Link ISIS-300 system (Oxford Microanalysis Group) equipped with a Si(Li) detector and an energy resolution of 133 eV. X-ray photoelectron spectroscopy (XPS) was performed on a Multilab 2000 (Thermo) spectrometer equipped with Al Kα anode (hν = 1486.6 eV). All spectra were referenced to the C 1s peak of adventitious carbon at 285.0 eV. For quantification purposes, survey at a pass energy of 50 eV and high-resolution spectra at pass energy of 20eV were recorded and analyzed by XPS Peak 4.1 software (written by Raymund Kwok). The spectra were decomposed assuming line shapes as sum functions of Gaussian (80 %) and Lorentzian (20 %) functions. Raw areas determined after subtraction of a Shirley background[13] were corrected according to following sensitivity factors[14] (C 1s: 0.25; N 1s: 0.42; O 1s: 0.66; Cl 2p: 0.73; Zn 3p: 0.75). Etching Ar+ bombardment was performed at 2 kV and 18 mA of ionic current.

Results and discussion

General considerations. The synthesis of graphitic carbon nitride (g-C_3N_4) usually starts from dicyandiamide (DCDA) and proceeds by a number of sequential condensation processes that occur between ~230 and 550 °C (Scheme 1a). We selected zinc chloride as a main component of the salt melt due to the two following reasons. First of all, $ZnCl_2$ is a moderate-strength Lewis acid and was expected to solubilize the precursor and at least some of the condensation intermediates owing to strong Lewis acid-base interactions. Besides, it has a low melting temperature that can even be lowered to $T_m < 300$°C in eutectic mixtures with alkali metal chlorides (see Table 1). On the other hand, melamine was chosen as a carbon nitride precursor due to the fact that its condensation temperature towards melam is estimated to be roughly 335 °C[15] (Scheme 1a). That way, we hope to ensure melting of the solvent before the onset of the melamine condensation reaction.

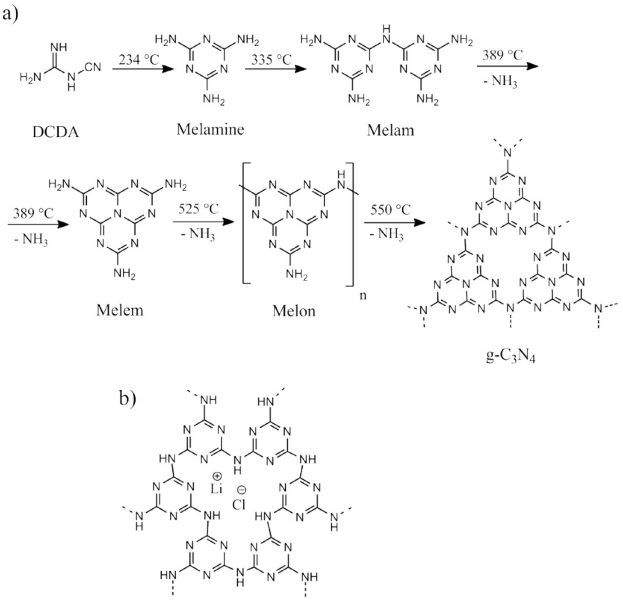

Scheme 1. a) Idealized condensation scheme of dicyandiamide (DCDA) to graphitic carbon nitride; b) idealized structure of poly(triazine imide)/Li^+Cl^- [16].

Table 1. Composition and melting points of eutectic salt mixtures used in this paper.

Salt mixture A/B(/C)	A content, wt. %	B content, wt. %	C content, wt. %	Molar content of $ZnCl_2$	Melting Temperature, °C[17]
$ZnCl_2$	100	-	-	1.00	318
$LiCl/ZnCl_2$	8.5	91.5	-	0.770	294
$NaCl/ZnCl_2$	23.7	76.3	-	0.580	270
$KCl/ZnCl_2$	36.3	63.7	-	0.490	230
$CsCl/ZnCl_2$	48.3	51.7	-	0.575	263
$NaCl/KCl/ZnCl_2$	10.7	13.8	75.5	0.600	203

Initial investigations were conducted at a fixed precursor to salt mixture ratio (1:5 by weight), while the composition of the salt mixture was varied by choosing different alkali metal chlorides.

The synthesis and work-up procedure yielded colored products, which were analyzed by EA, EDX and XPS with regard to their composition (Table 2). The C/N weight ratios in the products range from 0.59 to 0.61 and are slightly higher than the value

for reference g-C_3N_4 (0.58) but slightly lower than the stoichiometric value for C_3N_4 (0.64). This might be explained by incomplete amide condensation and the corresponding presence of terminal NH/NH_2-groups. The sum of C, N, and H as obtained from EA is typically lower than 100%, usually around 82-87%. The remaining 13-18 wt.% are Zn (3-5%), O (10-15%) and Cl (1-3%) ions as analyzed by EDX spectroscopy and XPS for selected samples. Zinc could be removed completely by washing the composites with 10M HCl. This step is however accompanied by additional protonation of the product surface[18] and was hence not employed in the default recipe. The presence of oxygen in products is partially the result of the aqueous work-up of the reaction mixtures but also due to the strong adsorption of water and CO_2 under ambient conditions.

Table 2. Composition of materials synthesized in different $ZnCl_2$ containing salt melts (EA data), and calculated BET surface areas of products.

Melt	C, wt.%	N, wt.%	H, wt.%	C/N wt.	100-(C+N+H)	Color	S_{BET} m^2/g
Ref. bulk C_3N_4	35.0	60.1	2.06	0.58	2.8	yellow	10
$LiCl/ZnCl_2$	30.6	50.8	2.70	0.60	15.9	pale yellow	20
$NaCl/ZnCl_2$	29.6	49.1	3.04	0.60	18.3	brown	193
$KCl/ZnCl_2$	30.1	49.2	3.06	0.61	16.0	yellow	42
$CsCl/ZnCl_2$	30.2	49.8	3.13	0.59	16.5	yellow	68
$NaCl/KCl/ZnCl_2$	29.7	50.3	3.13	0.59	16.9	brown	71
Pure $ZnCl_2$	31.5	52.5	2.86	0.60	13.1	pale yellow	58

XRD and FTIR spectroscopy investigations showed that the synthesized materials have features typically observed for previously described carbon nitride polymers, but differ from each other with respect to the degree of structural order. Figure 1a illustrates that products prepared in $NaCl/ZnCl_2$, $CsCl/ZnCl_2$ and $NaCl/KCl/ZnCl_2$ eutectics are mostly X-ray amorphous as they show only broad halos at 2θ ~ 15° and 27°, $LiCl/ZnCl_2$-derived material shows quite defined reflections corresponding to higher crystallinity, while the product obtained from pure $ZnCl_2$ is characterized by outstanding structural order. The main 2θ reflection around 27° is present in the diffractograms of all materials and corresponds to interplanar stacking of carbon nitride layers. Another reflection observed for most of the materials (except for $NaCl/KCl/ZnCl_2$ and $NaCl/ZnCl_2$ eutectics) at 2θ ~12-15° is related to in-plane structural packing motifs. The appearance of XRD patterns of products prepared in $ZnCl_2$ and $LiCl/ZnCl_2$ suggests that these materials are poly(triazine imide)-like as corroborated by recent investigations of acid washed poly(triazine imides) obtained from LiCl/KCl[19]. $KCl/ZnCl_2$-derived material seems to be composed of two phases characterized by different crystallinity. In principle, crystallinity of carbon nitrides prepared in different $ZnCl_2$-containing melts increases in the row $NaCl/KCl/ZnCl_2$ ~ $NaCl/ZnCl_2$ < $CsCl/ZnCl_2$ < $KCl/ZnCl_2$ < $LiCl/ZnCl_2$ < bulk g-C_3N_4 < $ZnCl_2$, and therefore can be tuned by varying the nature of the salt eutectic used for the synthesis. Figure 1b shows that the main IR absorption bands displayed by the synthesized materials are similar to those of reference g-C_3N_4. Namely, the large absorption band at 1200-1650 cm^{-1} corresponds to stretching vibrations of CN heterocycles, a strong vibration at ~800 cm^{-1} is attributed to deformation vibrations of triazine or tri-*s*-triazine ring, and the broad band between 2400 and 3400 cm^{-1} indicates stretching vibrations of surface hydroxyl groups (OH-) and terminal and residual amino-groups (NH_2-, NH-). The presence of the distinct absorption band at ~1350 cm^{-1} in $ZnCl_2$-, $LiCl/ZnCl_2$- and $KCl/ZnCl_2$-derived materials suggests that they are built of triazine rather than of tri-*s*-triazine rings[20] that is in good agreement with the XRD data. Besides, the amorphous nature of $NaCl/ZnCl_2$, $CsCl/ZnCl_2$ and $NaCl/KCl/ZnCl_2$-derived products causes broadening and subsequent overlap of the absorption bands, while improved structural order (products from pure $ZnCl_2$, $LiCl/ZnCl_2$ and $KCl/ZnCl_2$) results in more defined vibration peaks.

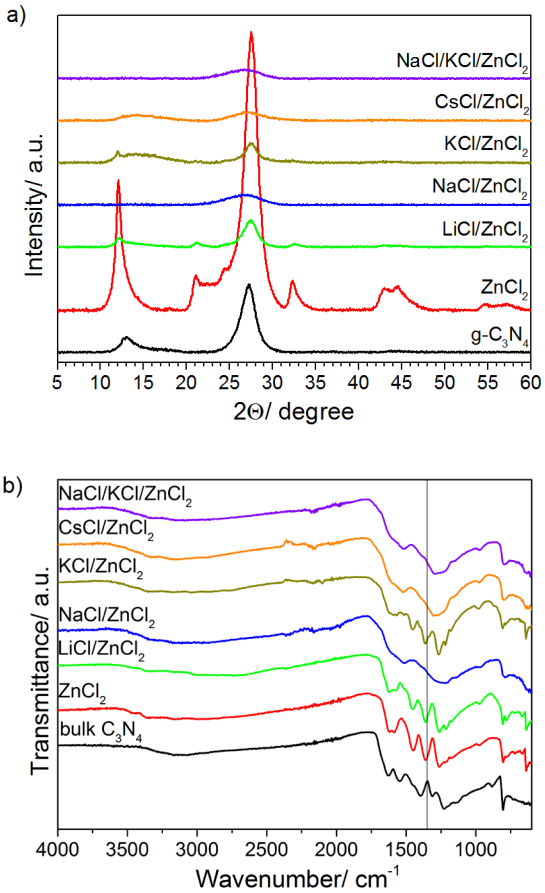

Figure 1. a) WAXS patterns and b) FTIR spectra of bulk-C_3N_4 and products synthesized in salt melts containing $ZnCl_2$. Vertical line indicates 1350 cm^{-1} position.

Amorphous $CsCl/ZnCl_2$-C_3N_4 sample was investigated by XPS in order to unravel the structure of the carbon nitride polymer and intercalated Zn^{2+} species. The C1s spectrum (Figure 2a) shows a main carbon species with a binding energy of 288.2 eV corresponding to CN_3 bonds[21]. In addition to the C1s peak of adventitious carbon at 185.0 eV, there is a weak peak at 283.3 eV which results from carbide impurities in the sample. The deconvolution of the N1s signal reveals three contributions (Figure 2b): at 401.2 eV (NH_x groups), 399.7 eV (C-N=C) and 397.6 eV (deprotonated N-sites). The number of contributions as well as their chemical shifts matches the calculated values

for N1s electrons in PTI prepared in LiCl/KCl[22]. The C/N ratio is then calculated as a ratio of the area of the main carbon peak to the total area of nitrogen peaks. The value of 0.59 fits the one for poly(triazine-imide) reported by Wirnhier et al.[10a] and differs from fully condensed heptazine-based C_3N_4 (0.64). Furthermore, the ratio of amino-nitrogen atoms (NH_x groups) to ring nitrogen atoms (C-N=C) calculated as a ratio of the corresponding peak areas, is equal to 0.49 and is close to the theoretical value of 0.5 for the idealized structure of PTI ($(C_3N_3)_2(NH)_3$). For heptazine-based structure this value would be much lower because only uncondensed terminal amino-groups would contribute to the XPS spectrum and only weak peaks for $-NH_x$ are reported for this case[21]. All these findings prove that the carbon nitride component of the composite is based on poly(triazine imide).

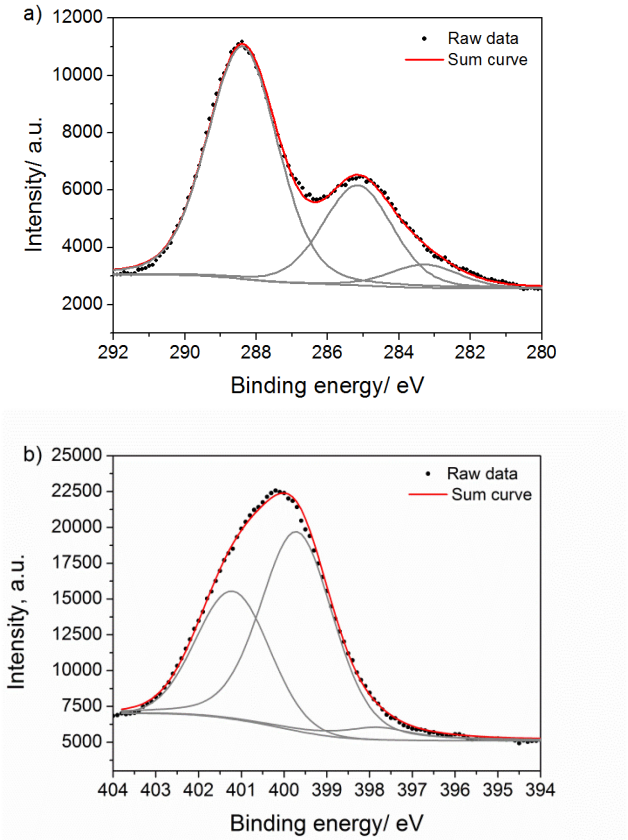

Figure 2. a) C1s and b) N1s XPS spectra of carbon nitride synthesized in $CsCl/ZnCl_2$.

XPS investigations further confirmed the presence of O, Zn and Cl in the sample. O1s signal (Figure S1a) consists of three contributions: at 529.3 eV (assigned to O-Zn bonds[23]), 531.5 eV (-OH groups)[24] and 533.0 eV (adsorbed water)[25]. The ratio between these three contributions is 1:16:8. The presence of Zn-O bonds is further confirmed by Zn3p signal (Figure S1b) which shows two main and almost equal contributions: at 88.4 eV for Zn-O bonds[26] and at 89.6 eV for Zn-Cl and Zn-OH bonds. The peak of Cl2p (Figure S1c) at 198.1 eV, by-turn, indicates the presence of Zn-Cl bonds. Basing on these findings, we conclude that the intercalated Zn species are mainly zinc oxide and zinc oxychloride. The latter one is the product of hydrolysis of $ZnCl_2$ during the work-up procedure. The qualitative differences between surface and bulk of the product were analyzed by comparing the XPS spectra before and after Ar-ion bombardment of the sample which allows removing the surface layer of the material. The Cl2p signal after ion bombardment reveals two peaks that correspond to different Zn-Cl bonds (Figure S2a). The contribution at 198.2 eV is due to zinc oxychloride while the one at 199.5 eV indicates the presence of zinc chloride[27] which didn't hydrolyze being entrapped in the structure. The presence of $ZnCl_2$ in the bulk of the product is also supported by Zn3p signal (Figure S2b) which shows now an additional contribution at 91.4 eV due to Cl-Zn-Cl bonds. The amount of zinc oxychloride in the bulk of the product is much higher than the amount of zinc oxide, though at the surface their quantities were almost even. This finding together with the fact that the amount of Zn in the bulk of the material is at least 3 times higher than at the surface illustrates the difficulty to remove the intercalated Zn species ascribed to the diffusion limitations. In contrast, the oxygen content in the bulk of the product is at least two times lower than at the surface that is explained by the removal of surface hydroxyl groups and surface-adsorbed water. The weight content of the elements calculated from XPS data is in good agreement with the values obtained from EA, ICP and EDX measurements (Table S1).

The morphology of the prepared materials was investigated by SEM. It was found to be fairly homogeneous within each of the samples and variant depending on the nature of alkali metal chloride constituting the salt melt (Figure 3). Carbon nitrides are obtained as crystalline densely-packed nanosheets of 100-200 nm in diameter from pure $ZnCl_2$ and $LiCl/ZnCl_2$ eutectic melts. $NaCl/ZnCl_2$, $CsCl/ZnCl_2$ and $NaCl/KCl/ZnCl_2$ melts give amorphous nanoparticles with the diameters of 50 ± 10 nm, 60 ± 10 nm and 40 ± 10 nm, respectively. $KCl/ZnCl_2$ eutectic gives rise to the mixed product morphology containing larger sheets (1-2 µm in diameter), and spherical nanoparticles aggregates (~300 nm in diameter).

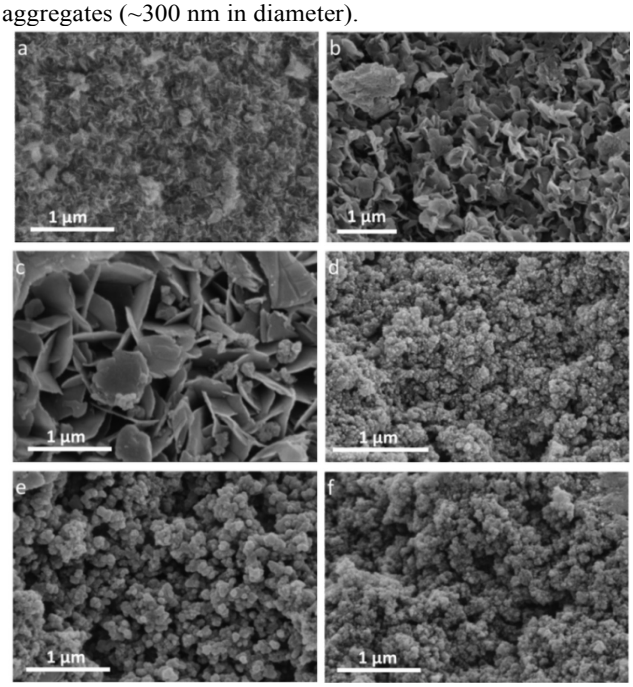

Figure 3. Representative SEM images of carbon nitrides synthesized in a) $ZnCl_2$, b) $LiCl/ZnCl_2$, c) $KCl/ZnCl_2$, d) $NaCl/ZnCl_2$, e) $CsCl/ZnCl_2$ and f) $NaCl/KCl/ZnCl_2$.

$ZnCl_2$ salt melt derived materials have higher specific surface areas as determined by Brunauer-Emmett-Teller (BET) analysis of the gas adsorption data compared to the reference g-C_3N_4 (see Table 1). However, the values are much lower than those reported for other types of materials prepared in $ZnCl_2$ melts (CTFs[11] and carbons[12]). The appearance of nitrogen adsorption/desorption isotherms suggests the absence of any kind of inner porosity in final MCl/$ZnCl_2$-C_3N_4 products, which is typical for carbon nitrides prepared in salt melts[10a]. Hence the estimated surface area values are reflecting only the external surface area of material particles, in good agreement with the results of SEM investigations.

The structural order and morphology of the products seem to correlate with the amount (χ) of $ZnCl_2$ in the salt melt at a fixed melamine to salt weight ratio (1:5) (see Table 1). Thus, at $\chi(ZnCl_2)$~0.6, products are obtained as amorphous spherical nanoparticles. Being a strong Lewis acid, $ZnCl_2$ interacts with cyano-groups of precursors and intermediates. This interaction facilitates their solubilization in the salt melt, but is also the source of the discussed structural complexity. The second component of the salt mixture (MCl, M=Li^+, Na^+, K^+, Cs^+) allows tuning the solubility of the reaction intermediates in the salt melt and thus influences the onset of "polymer – salt melt" phase separation. Li^+ and K^+ cations favor the solubilization of the reaction intermediates that results in slower phase separation and allow the growth of crystalline poly(triazine imides). Na^+ and Cs^+ seem to cause rather quick supersaturation of the melt with oligomeric intermediates that leads to the formation of numerous amorphous nanoparticles, which cannot crystallize into more extended networks.

Influence of synthesis parameters. In order to control morphology and crystallinity of salt melt derived carbon nitrides, the influence of various reaction parameters on product properties was studied using NaCl/$ZnCl_2$ as an example eutectic. Among these are synthesis temperatures (400, 450, 500, 550, 600 °C) (Fig. S3, Tables S2, S3), heating rates (2.5, 5, 10, 20, 40 °C/min) (Fig. S4, Table S4), holding times (2, 4, 6, 8, 10 hours) (Fig. S5, Table S5), precursor to salt ratios (1:1, 1:2, 1:5, 1:10, 1:20) (Fig. S6, Table S6), synthesis atmospheres (N_2, air, ampoule) and type of C_3N_4 precursors (DCDA, melamine). The results of these studies are briefly discussed below, but for more detailed information the reader is referred to the Supporting Information.

We found that the microstructure of products is mainly defined already at 400 °C. This means that the final morphology is determined by precipitation and crystallization of intermediary condensates at the point of vanishing solubility in the salt melt. No significant changes in FTIR spectra and WAXS diffractograms can be observed when the synthesis temperature is further increased from 400 to 600 °C (Figure S3). However, the degree of condensation of the polymeric networks increases with raising the reaction temperature, resulting in slightly improved C/N ratios (0.59 to 0.61) and narrowing the band gap of the resulting semiconductors, as already visually observed as an intensification of products colors. In the case of applying a one-step heating procedure (Scheme S1b), materials obtained at 550 °C are characterized by slightly higher values of the BET surface areas if compared to those synthesized at 600 °C (144 and 115 m^2/g, respectively) while providing the same C/N ratio (0.61, Table S3), thus 550 °C was selected as the temperature of choice for running the condensation. This is in good agreement with previous observations however on bulk condensation of C_3N_4 precursors.

Variations of the heating rate and holding time (Fig. S4, S5) have only minor influence on products structures, though the best products compositions characterized by a C/N ratio of 0.61 were obtained at 10 °/min ramp and 6 hours holding time. Other studied parameters gave lower C/N ratios in the products (Tables S4, S5).

As the morphology is given by a product precipitation at rather early stages of the condensation, the concentration of the precursor in the melt must have crucial impact on the morphology and crystallinity of $ZnCl_2$-derived carbon nitrides. Here, three different regimes were established: both low (1:1 precursor to salts weight ratio) and high (1:10, 1:20 wt. ratios) melamine concentrations give highly crystalline products, while concentrations in between (1:2, 1:5 wt. ratios) lead rather to amorphous polymeric structures (Figure S7). The crystalline species have sheet-like morphology characterized by different diameters: 0.3-1 μm for 1:1 ratio, 1.5-2 μm for 1:10, and 50-80 nm for 1:20. The intermediary concentrations form nanoparticles 50-100 nm in size (Figure 4). The BET surface areas of products after acidic work-up vary between 60 and 190 m^2/g (Table S6).

We can only speculate about the origin of this morphology changes. We suggest that at high precursor concentrations, a molecular complex between melamine and $ZnCl_2$ is initially formed, which consumes all $ZnCl_2$. Further transformations do not occur in a solution anymore but in solid state, and rather the structure of complexes between $ZnCl_2$ and intermediates determines the high order in the final products. Upon decreasing melamine concentration, the initially formed molecular complex is redissolved at higher temperatures, but while polymerizing quickly reaches supersaturation and precipitates as amorphous nanoparticles. In some cases (NaCl/$ZnCl_2$, CsCl/$ZnCl_2$, NaCl/KCl/$ZnCl_2$) even spinodal decomposition of the polymer/salt melt phase is assumed to take place, yielding highly microporous materials (see below). At low precursor concentration, demixing of phases occurs slowly, and the polymer (PTI) has enough time to crystallize. It ejects the solvent because the cohesion energy of carbon nitride is higher than the secondary valence to the metal center.

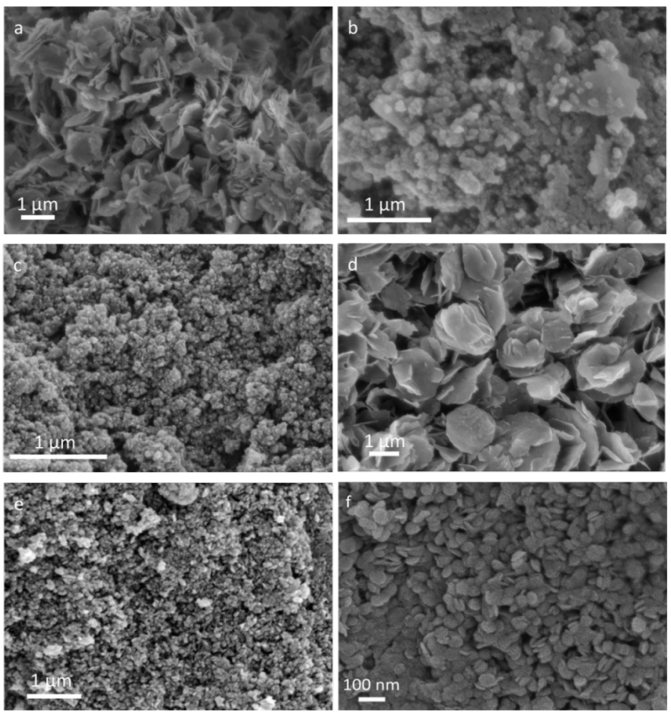

Figure 4. SEM images of materials synthesized in NaCl/$ZnCl_2$ salt melts using different precursor to salt ratios: a) 1:1, b) 1:2, c) 1:5, d) 1:10, e), f) 1:20.

Products prepared in pure $ZnCl_2$. In order to elaborate on the reactive nature of pure $ZnCl_2$ and the role of the second component of the eutectic salt mixture to moderate this reactivity, we also investigated the condensation of melamine in pure $ZnCl_2$ at different precursor concentrations. Materials derived from pure $ZnCl_2$ melts have typically dense structures with heterogeneous morphologies, which complicate the removal of the intercalated Zn ions, especially at low precursor to salt ratios (1:1, 1:2). Some illustrative SEM images of products obtained from $ZnCl_2$ melts at different precursor concentrations are shown in Figure 5, while Figure S7a presents typical WAXS patterns of composites. Similar to NaCl/$ZnCl_2$ eutectic, three regimes determining the product morphology and crystallinity are observed. At 1:1 ratio, both nanoparticle and nanosheet morphologies can be recognized, at 1:2 ratio the resulting material is obtained as amorphous spherical nanoparticles, while at 1:5 and 1:10 ratios the products are mostly crystalline, organized into sheet-like structures covering broad range of shapes and dimensions (from the nano- to microrange). As a consequence, the BET surface areas of those products are typically low.

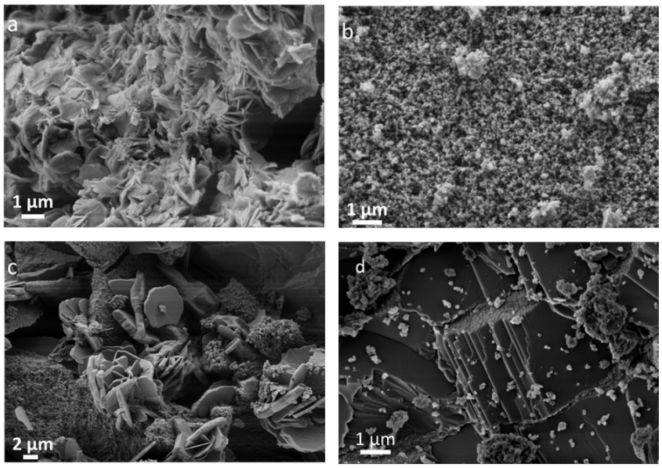

Figure 5. Selected SEM images of materials synthesized in $ZnCl_2$ using different precursor to salt ratios: a) 1:1, b) 1:2, c) 1:5, d) 1:10.

Due to the very strong donor-acceptor interactions of $ZnCl_2$ with the precursor, zinc cyanamide (also called zinc carbodiimide, $Zn(CN_2)$) is formed as a by-product when performing the reaction in pure $ZnCl_2$. At 1:10 precursor to salt ratio, the yield of $ZnCN_2$ is ~50 %. When the ratio is further lowered down to 1:20, solely $ZnCN_2$ is formed (Figure S7a and b). These results prove the precoordination between the salt and the monomer via N-Zn donor-acceptor bonds formation and point out the alternative reaction pathway in the case of $ZnCl_2$ if compared to LiX/KX (X=Cl, Br) melts. LiX/KX melts only weakly solubilize poly(triazine imides), therefore phase demixing occurs early, and big crystalline structures can grow from that melts. On the contrary, strong binding of Zn to condensation intermediates ensures their solubilization, and at later condensation stages the reaction progresses towards the thermodynamically more stable $Zn(CN_2)$ rather than to C_3N_4. Thus, $ZnCl_2$ should be always considered as a reactive solvent in the case of carbon nitride synthesis.

$Zn(CN_2)$ can be easily removed by washing the product mixture with diluted acid, or converted to zinc oxide by re-heating the composite in air (2 hours at 400 °C; note that contrary to carbon nitride $Zn(CN_2)$ is not oxidation stable). In this way, PTI/ZnO composites can be obtained. Figure 6 shows a TEM image and SAED pattern of such a composite containing ~40 wt.% C_3N_4 and ~60 wt.% ZnO (crystallite size: 13±2 nm) and having a BET surface area of 270 m^2/g (Figure S8). The photocatalytic activity of this material is discussed below.

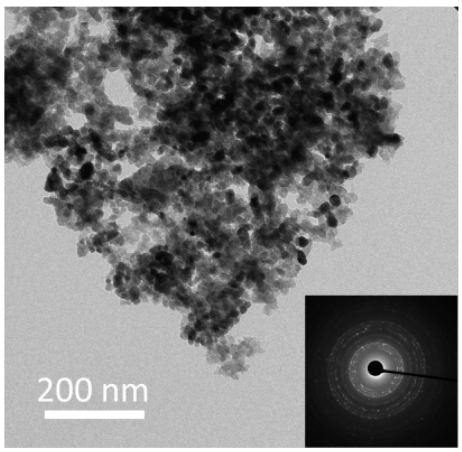

Figure 6. TEM image and SAED pattern of PTI/ZnO composite.

Optical absorption and emission properties of $ZnCl_2$-derived carbon nitrides are compared with those of g-C_3N_4 in Figure 7a and 7b, respectively. As it can be seen, NaCl/$ZnCl_2$- and CsCl/$ZnCl_2$-derived materials absorb visible light over a wide wavelength range. If compared to g-C_3N_4, the absorption band edge of these composites is obviously smeared to longer wavelengths. The appearance of the absorption spectra of NaCl/$ZnCl_2$-C_3N_4, CsCl/ $ZnCl_2$-C_3N_4 and PTI/ZnO composite (Figure S9) is typical for dyade materials, such as carbon@TiO_2[28]. In a dyade, two components form a joint electronic system, and the altered absorption spectrum likely points out at charge transfer between carbon nitride and Zn containing species (such as ZnO). At the same time, the steady state photoluminescence of the products from NaCl/$ZnCl_2$ and CsCl/$ZnCl_2$ excited at 300 nm is negligible, that implies that the relaxation of excitons occurs via non-radiative pathways: charge transfer at heterojunction and/or non-radiative recombination at the impurity states in the crystal lattice.

The product obtained from LiCl/$ZnCl_2$ melt on the other hand absorbs less visible light and is characterized by slightly stronger emission than g-C_3N_4. Both absorption and emission spectra indicate that this semiconductor has a wider band-gap compared to the reference carbon nitride. This is in good agreement with the assignment that this structure is based on triazine imide moieties, as previously reported salt melt products[19, 22]. The optical properties of the material synthesized in KCl/$ZnCl_2$ lie in between those of LiCl/$ZnCl_2$ and NaCl/$ZnCl_2$- or CsCl/$ZnCl_2$-derived composites, that is in agreement with XRD and SEM data discussed above.

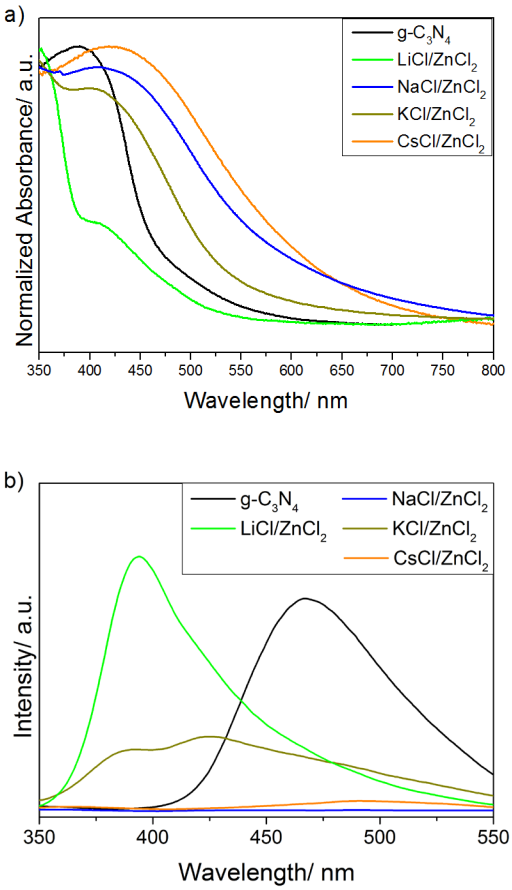

Figure 7. a) Visible light diffuse reflectance spectra and b) steady-state photoluminescence spectra of g-C_3N_4 and MCl/$ZnCl_2$-C_3N_4 (M=Li, Na, K, Cs); excited at 300 nm.

Composites obtained after only aqueous work-up of the reaction mixtures. Materials, which were only washed with water, but not with 1M HCl showed a C/N weight ratio of 0.70-0.85. This suggests the formation of some carbonaceous species other than C_3N_4 (*e.g.* $ZnCO_3$). This goes along with an overall low content of C, N, H (sum: 40-50 wt.%) and the presence of other elements. Small amounts of zinc cyanamide, zinc cyanide and zinc oxychloride might also be present, according to XRD studies (Figure S10). Acid washing step efficiently removes all these by-products, so that the final C/N ratio is ~0.6 again, as mentioned above (Table S7).

The water-washed MCl/$ZnCl_2$-derived composites typically possess higher specific surface areas than the acid-treated ones. The most striking example is NaCl/$ZnCl_2$-C_3N_4, whose BET surface area dropped from 700 m^2/g (value after water washing) to 193 m^2/g after the acidic treatment (Figure S11). Such behavior may be explained by the collapse of the internal structure during acidic work-up or the removal of high surface area impurities, such as nanoparticles onto the hybrid. In the first case, the composite material after water washing may be envisaged as a poor, amorphous analogue of metal organic frameworks, in which triazine imide (oligomeric) moieties play the role of organic ligands, which are interconnected by Zn^{2+} ions, $ZnCl_2$, ZnO clusters, or other species. Such microporous

composite materials show very promising adsorption properties, which will be discussed later.

Applications. Among *potential applications* for at least some of $ZnCl_2$-derived carbon nitride composites, we would like to underline the following two: CO_2 adsorbents and photocatalysts.

The highly microporous NaCl/$ZnCl_2$-derived C_3N_4 composite (water-washed only) was investigated with respect to its CO_2 adsorption properties (Figure 8 and S12, S13). It shows quite high CO_2 uptake of 3.6 mmol/g at 0°C and 2.5 mmol/g at 30°C. The steep rise of the amount of adsorbed CO_2 at low pressures indicates the presence of rather small micropores, which could indeed be interesting for separation applications. The N_2 uptake at 0°C and 30°C was also studied and initial calculation with respect to the CO_2/N_2 selectivity α were undertaken. Ideal adsorbed solution theory (IAST)[29] gives α = 225 (0°C) and α = 100 (30°C) at 1 bar and a gas composition of CO_2 /N_2 of 0.15/0.85 that reflects an approximate composition of a flue gas. Such selectivities are indeed competitive to some reported zeolites[30] and MOFs[31] given also the simplicity of synthesis and purification procedures as well as the relatively high product yield of 50 % (based on total C content in the precursor and the product).

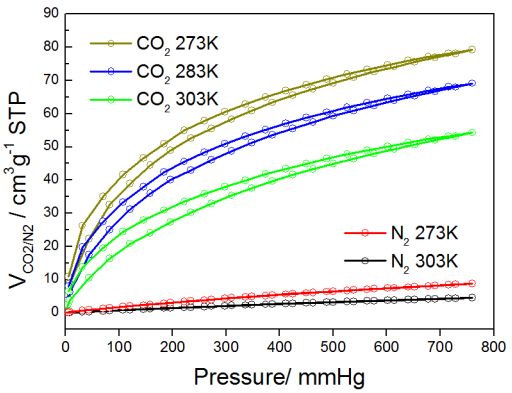

Figure 8. CO_2 and N_2 adsorption-desorption isotherms of microporous NaCl/$ZnCl_2$-derived C_3N_4 composite (after water washing step).

The *photocatalytic properties* of $ZnCl_2$-derived carbon nitrides were evaluated in a model reaction assay, the photodegradation of Rhodamine B (RhB) under blue light (λ=420 nm) irradiation. Here, two selected examples of remarkable performance are the microporous NaCl/$ZnCl_2$-derived C_3N_4 hybrid (water-washed), again, and the C_3N_4/ZnO (40 wt.%/60 wt.%) nanocomposite. The estimated rate constants of RhB degradation accomplished by these two photocatalysts are k_0=21·10^{-3} min^{-1} and k_0=12·10^{-3} min^{-1}, respectively; these are ~10 and ~5 times higher than the one observed for the reference g-C_3N_4 (2.2·10^{-3} min^{-1}). We mainly attribute these enhanced activities to the increased surface areas of the composites and improved absorption of visible light due to the formation of the dyadic structures. Additionally, the C_3N_4/ZnO hybrid is characterized by an improved crystallinity of ZnO NPs that results in better transport of the photo-generated and transferred electrons to the surface-adsorbed RhB and O_2 molecules.

Conclusions

In summary, condensation of melamine in $ZnCl_2$-containing eutectic salt melts gives rise to a broad range of novel carbon nitride-based composite materials with the improved absorption in visible light range due to the formation of dyadic system between C_3N_4 and ZnO clusters or other Zn^{2+} containing species. Unlike LiX/KX (X=Cl, Br), $ZnCl_2$ plays a role of the reactive solvent during the synthesis of carbon nitrides, and binds strongly to the condensation intermediates. Adjustment of precursor concentration and a proper selection of the alkali metal chloride constituent of MCl/$ZnCl_2$ melt give a possibility to change the on-set of phase demixing, tune the interactions strength between the condensation intermediates and the solvent and vary the solubility of the intermediates in the melt. Overall, one can direct the reaction from zinc cyanamide to both crystalline poly(triazine imides) or MOF-like hybrid materials. The latters have surface areas up to 700 m^2/g and turned out to be interesting as highly performing CO_2 adsorbents and photocatalysts.

Acknowledgements

The authors want to gratefully acknowledge the Max Planck Society, Dr. J. Hartmann for EDX measurements and Dr. G. Clavel for TEM measurements.

Notes and references

[a] Max-Planck Institute of Colloids and Interfaces, Department of Colloid Chemistry, Research Campus Golm, 14424 Potsdam, Germany. E-mail: dariya.dontsova@mpikg.mpg.de

[b] University of Applied Science Zittau/Görlitz, Department of Chemistry, 02763 Zittau, Germany.

† Electronic Supplementary Information (ESI) available: O1s, Zn3p and Cl2p XPS spectra of CsCl/$ZnCl_2$-C_3N_4, Schemes of Heating procedures; WAXS pattern, FTIR spectra, EA and surface areas of products synthesized at different temperatures, heating rates, holding times and ratios; WAXS pattern and FTIR spectra of materials made in pure $ZnCl_2$; diffuse reflectance spectra of NaCl/$ZnCl_2$-C_3N_4 and C_3N_4/ZnO composites, CO_2 and N_2 adsorption/desorption experimental isotherms and predictions of gas uptake of CO_2 and N_2 at 303 K, Rhodamine B degradation data. See DOI: 10.1039/b000000x/

1. (a) Wang, X.; Maeda, K.; Thomas, A.; Takanabe, K.; Xin, G.; Carlsson, J. M.; Domen, K.; Antonietti, M., *Nat. Mater.* **2009,** *8* (1), 76-80; (b) Maeda, K.; Wang, X.; Nishihara, Y.; Lu, D.; Antonietti, M.; Domen, K., *J. Phys. Chem. C* **2009,** *113* (12), 4940-4947.

2. Shalom, M.; Gimenez, S.; Schipper, F.; Herraiz-Cardona, I.; Bisquert, J.; Antonietti, M., *Angewandte Chemie* **2014,** *126* (14), 3728-3732.

3. (a) Wang, Y.; Zhang, J.; Wang, X.; Antonietti, M.; Li, H., *Angew. Chem.* **2010,** *122* (19), 3428-3431; (b) Wang, Y.; Di, Y.; Antonietti, M.; Li, H.; Chen, X.; Wang, X., *Chem. Mater.* **2010,** *22* (18), 5119-5121; (c) Wang, Y.; Li, H.; Yao, J.; Wang, X.; Antonietti, M., *Chem. Sci.* **2011,** *2* (3), 446-450; (d) Su, F.; Mathew, S. C.; Lipner, G.; Fu, X.; Antonietti, M.; Blechert, S.; Wang, X., *J. Am. Chem. Soc.* **2010,** *132* (46), 16299-16301.

4. Naffakh, M.; López, V.; Zamora, F.; Gómez, M. A., *Soft Materials* **2010,** *8* (4), 407-425.
5. (a) Zhang, Y.; Mori, T.; Niu, L.; Ye, J., *Energy Environ. Sci.* **2011,** *4* (11), 4517-4521; (b) Zhang, Y.; Mori, T.; Ye, J.; Antonietti, M., *J. Am. Chem. Soc.* **2010,** *132* (18), 6294-6295.
6. (a) Groenewolt, M.; Antonietti, M., *Adv. Mater.* **2005,** *17* (14), 1789-1792; (b) Kailasam, K.; Epping, J. D.; Thomas, A.; Losse, S.; Junge, H., *Energy Environ. Sci.* **2011,** *4* (11), 4668-4674; (c) Goettmann, F.; Fischer, A.; Antonietti, M.; Thomas, A., *Angew. Chem. Int. Ed.* **2006,** *45* (27), 4467-4471.
7. (a) Shalom, M.; Inal, S.; Fettkenhauer, C.; Neher, D.; Antonietti, M., *J. Am. Chem. Soc.* **2013,** *135* (19), 7118-7121; (b) Jun, Y.-S.; Lee, E. Z.; Wang, X.; Hong, W. H.; Stucky, G. D.; Thomas, A., *Adv. Funct. Mater.* **2013,** *23* (29), 3661-3667.
8. (a) Wang, Y.; Wang, X.; Antonietti, M.; Zhang, Y., *ChemSusChem* **2010,** *3* (4), 435-439; (b) Zhang, Y.; Schnepp, Z.; Cao, J.; Ouyang, S.; Li, Y.; Ye, J.; Liu, S., *Scientific reports* **2013,** *3*, 2163.
9. (a) Guo, Q.; Xie, Y.; Wang, X.; Lv, S.; Hou, T.; Liu, X., *Chem. Phys. Lett.* **2003,** *380* (1–2), 84-87; (b) Guo, Q.; Xie, Y.; Wang, X.; Zhang, S.; Hou, T.; Lv, S., *Chem. Comm.* **2004,** (1), 26-27.
10. (a) Wirnhier, E.; Döblinger, M.; Gunzelmann, D.; Senker, J.; Lotsch, B. V.; Schnick, W., *Chem. Eur. J.* **2011,** *17* (11), 3213-3221; (b) Chong, S. Y.; Jones, J. T. A.; Khimyak, Y. Z.; Cooper, A. I.; Thomas, A.; Antonietti, M.; Bojdys, M. J., *J. Mater. Chem. A* **2013,** *1* (4), 1102-1107.
11. (a) Kuhn, P.; Antonietti, M.; Thomas, A., *Angew. Chem. Int. Ed.* **2008,** *47* (18), 3450-3453; (b) Kuhn, P.; Forget, A.; Hartmann, J.; Thomas, A.; Antonietti, M., *Adv. Mater.* **2009,** *21* (8), 897-901; (c) Kuhn, P.; Thomas, A.; Antonietti, M., *Macromolecules* **2008,** *42* (1), 319-326.
12. Fechler, N.; Fellinger, T.-P.; Antonietti, M., *Adv. Mater* **2013,** *25* (1), 75-79.
13. Shirley, D. A., *Phys. Rev. B* **1972,** *5*.
14. Wagner, C. D.; Davis, L. E.; Zeller, M. V.; Taylor, J. A.; Raymond, R. H.; Gale, L. H., *Surf. Interface Anal.* **1981,** *3* (5), 211-225.
15. (a) Bojdys, M. J. Über neue Allotrope und Nanostrukturen von Karbonitriden. Universität Potsdam, Potsdam, 2009; (b) Lotsch, B. V.; Schnick, W., *Chem. Eur. J.* **2007,** *13* (17), 4956-4968.
16. Schwinghammer, K.; Tuffy, B.; Mesch, M. B.; Wirnhier, E.; Martineau, C.; Taulelle, F.; Schnick, W.; Senker, J.; Lotsch, B. V., *Angew. Chem. Int. Ed.* **2013**.
17. Janz, G. J.; Allen, C. B.; Downey Jr., J. R.; Tomkins, R. P. T., *Physical Properties Data Compilations Relevant to Energy Storage*. National Standard Reference Data System: New York, 1978.
18. Zhang, Y.; Thomas, A.; Antonietti, M.; Wang, X., *J. Am. Chem. Soc.* **2008,** *131* (1), 50-51.
19. Ham, Y.; Maeda, K.; Cha, D.; Takanabe, K.; Domen, K., *Chem. Asian J.* **2013,** *8* (1), 218-224.
20. Manecke, V. G.; Wöhrle, D., *Macromol. Chem. Phys.* **1968,** *120* (1), 176-191.
21. Thomas, A.; Fischer, A.; Goettmann, F.; Antonietti, M.; Muller, J.-O.; Schlogl, R.; Carlsson, J. M., *J. Mater. Chem.* **2008,** *18* (41), 4893-4908.
22. McDermott, E. J.; Wirnhier, E.; Schnick, W.; Virdi, K. S.; Scheu, C.; Kauffmann, Y.; Kaplan, W. D.; Kurmaev, E. Z.; Moewes, A., *J. Phys. Chem. C* **2013,** *117* (17), 8806-8812.
23. Biesinger, M. C.; Lau, L. W. M.; Gerson, A. R.; Smart, R. S. C., *Appl. Surf. Sci.* **2010,** *257* (3), 887-898.
24. Boshkov, N.; Petrov, K.; Vitkova, S.; Nemska, S.; Raichevsky, G., *Surf. Coat. Technol.* **2002,** *157* (2–3), 171-178.
25. Coppa, B. J.; Davis, R. F., *Appl. Phys. Lett.* **2003,** *82* (3), 400-402.
26. Strohmeier, B. R.; Hercules, D. M., *J. Catal.* **1984,** *86* (2), 266-279.
27. Klein, J. C.; Hercules, D. M., *J. Catal.* **1983,** *82*, 424-441.
28. Zhao, L.; Chen, X.; Wang, X.; Zhang, Y.; Wei, W.; Sun, Y.; Antonietti, M.; Titirici, M.-M., *Adv. Mater.* **2010,** *22* (30), 3317-3321.
29. Myers, A. L.; Prausnitz, J. M., *AlChE J.* **1965,** *11* (1), 121-127.
30. Akhtar, F.; Liu, Q.; Hedin, N.; Bergstrom, L., *Energy Environ. Sci.* **2012,** *5* (6), 7664-7673.
31. Sumida, K.; Rogow, D. L.; Mason, J. A.; McDonald, T. M.; Bloch, E. D.; Herm, Z. R.; Bae, T.-H.; Long, J. R., *Chem. Rev.* **2011,** *112* (2), 724-781.

The outcome of the ionothermal condensation of melamine in $ZnCl_2$-containing salt melts can be directed to poly(triazine imides), MOF-like hybrid materials or zinc cyanamide/C_3N_4 composites by careful selection of reaction conditions.